



# Seismological and structural constraints on the 2011–2013, $M_{\max}$ 4.6 seismic sequence at the south-eastern edge of the Calabrian arc (North-eastern Sicily, Italy)

Laura Cammarata<sup>a</sup>, Stefano Catalano<sup>b</sup>, Salvatore Gambino<sup>a,\*</sup>, Mimmo Palano<sup>a</sup>,  
Francesco Pavano<sup>b</sup>, Gino Romagnoli<sup>b</sup>, Antonio Scaltrito<sup>a</sup>, Giuseppe Tortorici<sup>b</sup>

<sup>a</sup> Istituto Nazionale di Geofisica e Vulcanologia, Sezione di Catania, P.zza Roma 2, I-95125 Catania, Italy

<sup>b</sup> Dipartimento di Scienze Biologiche, Geologiche e Ambientali, Università di Catania, Corso Italia 57, I-95129 Catania, Italy

## ARTICLE INFO

### Keywords:

Seismic swarm  
Multiplets  
Structural analysis  
Stress field  
Mantle fluids  
Calabrian arc

## ABSTRACT

Between June 2011 and September 2013, the Nebrodi Mountains region was affected by a seismic swarm consisting of > 2700 events with local magnitude  $1.3 \leq M_L \leq 4.6$  and located in the 5–9 km depth interval. The seismic swarm defines a seismogenetic volume elongated along the E–W direction and encompasses the NW–SE-oriented tectonic boundary between the Calabrian arc (north-eastward) and the Sicilide units (south-westward). By exploring the recent tectonic deformation and the seismic behavior of the region, this study aims at providing additional constraints on the seismogenetic faults at the southern termination of the Calabrian arc. Waveform similarities analysis allowed observing that ~45% of the whole dataset can be grouped into six different families of seismic events. Earthquake multiplet families are mainly located in the eastern part of the seismogenetic volume. We suggest that such a feature is responsive to the lateral lithological variations as highlighted by geology (at the surface) and P-wave seismic tomography (at depth of 10 km). Stress tensor inversions performed on FPSs indicate that the investigated region is currently subject to a nearly biaxial stress state in an extensional regime, such that crustal stretching occurs along both NW–SE and NE–SW directions. Accordingly, mesoscale fault geometries and kinematics analyses evidence that a younger normal faulting stress regime led to a tectonic negative inversion by replacing the pre-existing strike-slip one. Based on our results and findings reported in recent literature, we refer such a crustal stretching to mantle upwelling process (as evidenced by diffuse mantle-derived gas emissions) coupled with a tectonic uplift involving north-eastern Sicily since Middle Pleistocene. Moreover, seismic swarms striking the region would be related to the migration of mantle and sub-crustal fluids toward the surface along the complex network of tectonic structures cutting the crust and acting as pathways.

## 1. Introduction

North-eastern Sicily, located at the southern termination of the Calabrian arc (Fig. 1), is characterized by the occurrence of temporally protracted seismic swarms. These swarms comprise small-to-moderate earthquakes and often involve shallow crustal volumes, exhibiting normal faulting features and appearing related to pore pressure transients by mantle fluid flows (e.g. Scarfi et al., 2005; Giammanco et al., 2008; Camarda et al., 2016). Here, we focus on a seismic swarm that began in June 2011 and lasted until September 2013, cumulating > 2500 events with local magnitude  $1.3 \leq M_L \leq 4.6$ . The north-eastern off-shore area was struck by a  $M_L = 5.6$  earthquake in April 1978 while the  $M_L = 4.6$  earthquake represents the largest earthquake striking the area in the instrumental age (Rovida et al., 2011). Moreover, in

historical times, such area has experienced the occurrence of two destructive earthquakes in 1613 and in 1739 (Rovida et al., 2011), whose seismogenetic sources are still debated. In this regards, the main challenge of this study is to explore the recent tectonic deformation stages and the seismic behavior of the study area by comparing structural data from field geology with the high-resolution spatial distribution and kinematics of the whole seismic swarm, in order to provide additional constraints on the seismogenetic faults that bound the southern termination of the Calabrian arc. The seismic events data have been collected by the INGV permanent seismic network that, since 29 June 2011, has been integrated with a mobile network consisting of 3 stations (see Cammarata et al., 2014 for additional details). In the same area, recent studies have outlined an updated morphotectonic setting of the region, highlighting a dominant NE–SW-oriented crustal stretching pattern,

\* Corresponding author.

E-mail address: [salvatore.gambino@ingv.it](mailto:salvatore.gambino@ingv.it) (S. Gambino).

<https://doi.org/10.1016/j.tecto.2017.11.021>

Received 7 June 2017; Received in revised form 13 November 2017; Accepted 16 November 2017

Available online 21 November 2017

0040-1951/ © 2017 Elsevier B.V. All rights reserved.





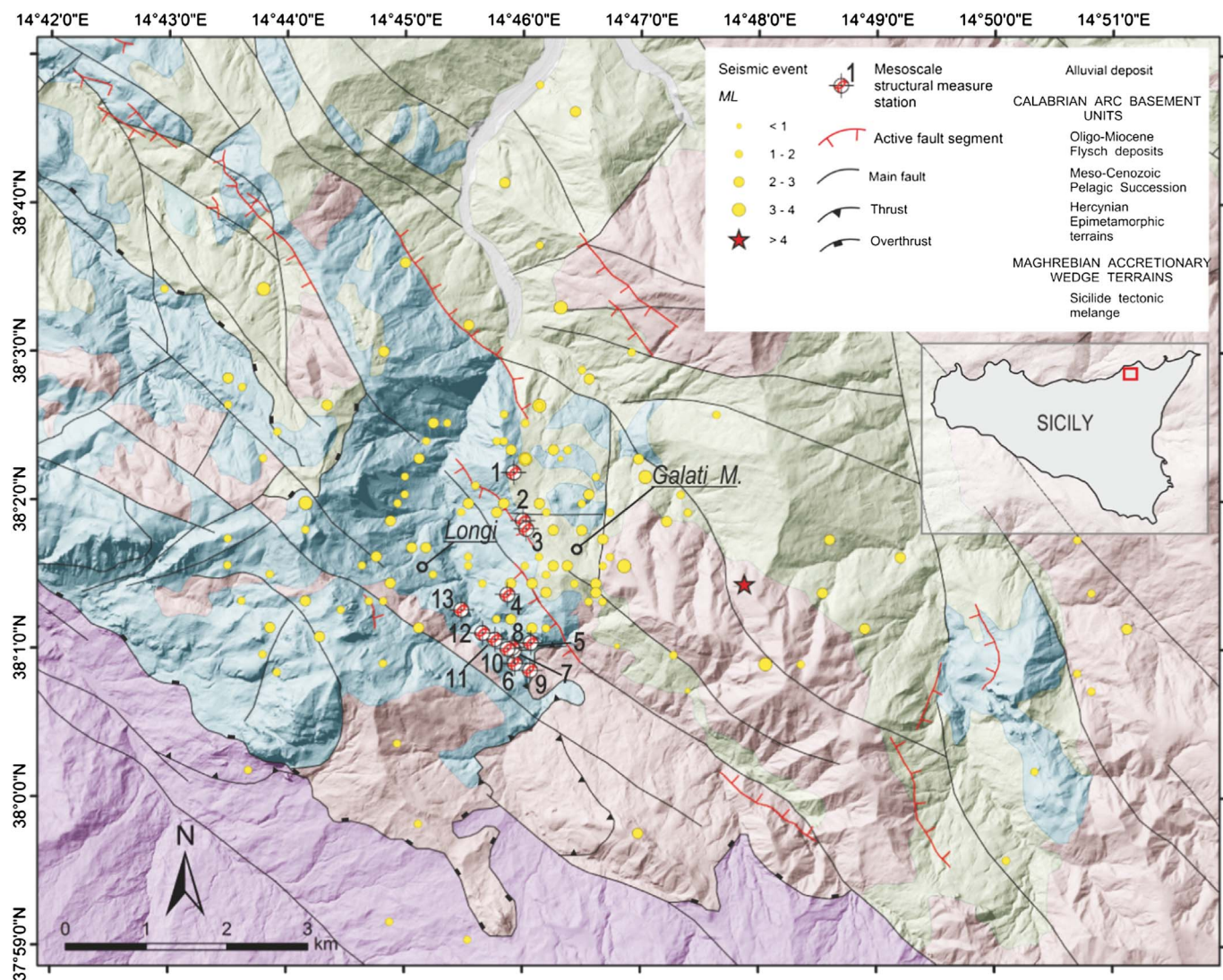


Fig. 2. a) Geological map of the region affected by the 2011–2013 seismic swarm, showing the main geological units and structural features. The standard location of the hypocentres of the analyzed seismic events, the position of the main shock (red star) and the distribution of the structural measure stations are also reported. (For interpretation of the references to colour in this figure legend, the reader is referred to the web version of this article.)

signatures consisting of the vertical displacement of Late Quaternary marine terraces (Catalano and Cinque, 1995; Catalano and Di Stefano, 1997; Pavano et al., 2015) and of the development of triangular facets and impressive dissection of raised landscapes (Pavano et al., 2015).

The main historical seismicity of north-eastern Sicily includes several historical moderate to large magnitude earthquakes (1172, 1613, 1739, 1780, 1786, 1908 CE; Postpischl, 1985; Mariotti, 1995; Boschi et al., 1997; Guidoboni et al., 2007; Rovida et al., 2011), the latest of which struck the Messina Strait area in the 1908 (Messina earthquake,  $M = 7.2$ ; Cello et al., 1982). In particular, the region of the 2011 seismic swarm was affected by two important historical earthquakes that occurred in the XVII (1613 CE) and XVIII centuries (1739 CE). Moment magnitudes of about 5.6 and 5.1 have been estimated for the two earthquakes, respectively (Rovida et al., 2011). However, the attribution of these events to any well-defined seismogenic fault is still debated.

### 3. Seismic data

#### 3.1. Seismic network

Since the early 2000's, continuous monitoring of the seismic activity

of eastern Sicily and southern Calabria has been performed initially by the local network installed in the framework of the "Poseidon Project", later merged into the Istituto Nazionale di Geofisica e Vulcanologia in 2001. The network consisted of a few analogic stations, equipped with three component short-period seismometers. Since 2003, the network was considerably enhanced, on one hand, with new seismic stations (Fig. 1), and on the other, by replacing the old analogic station with digital 24-bit ones, equipped with broadband (40s) three-component sensors, with a dynamic range of 144 dB.

In order to improve location accuracy of the seismic swarm, a mobile seismic network of 3 stations was installed close to Naso and Longi villages (Fig. 1) after the 23 June 2011 main-shock (Cammarata et al., 2014). This network worked from 29 June up to the end of September 2011.

#### 3.2. The seismic swarm

The investigated seismic swarm (Fig. 2) began in June 2011 and protracted with minor energy in 2012 and 2013. The seismic activity of 2011 lasted > 4 months between June and October, during which we recorded > 2500 events with local magnitude  $M_L \geq 1.3$ . The main event took place on 23 June 2011 at 22:02 (all times are in GMT), with

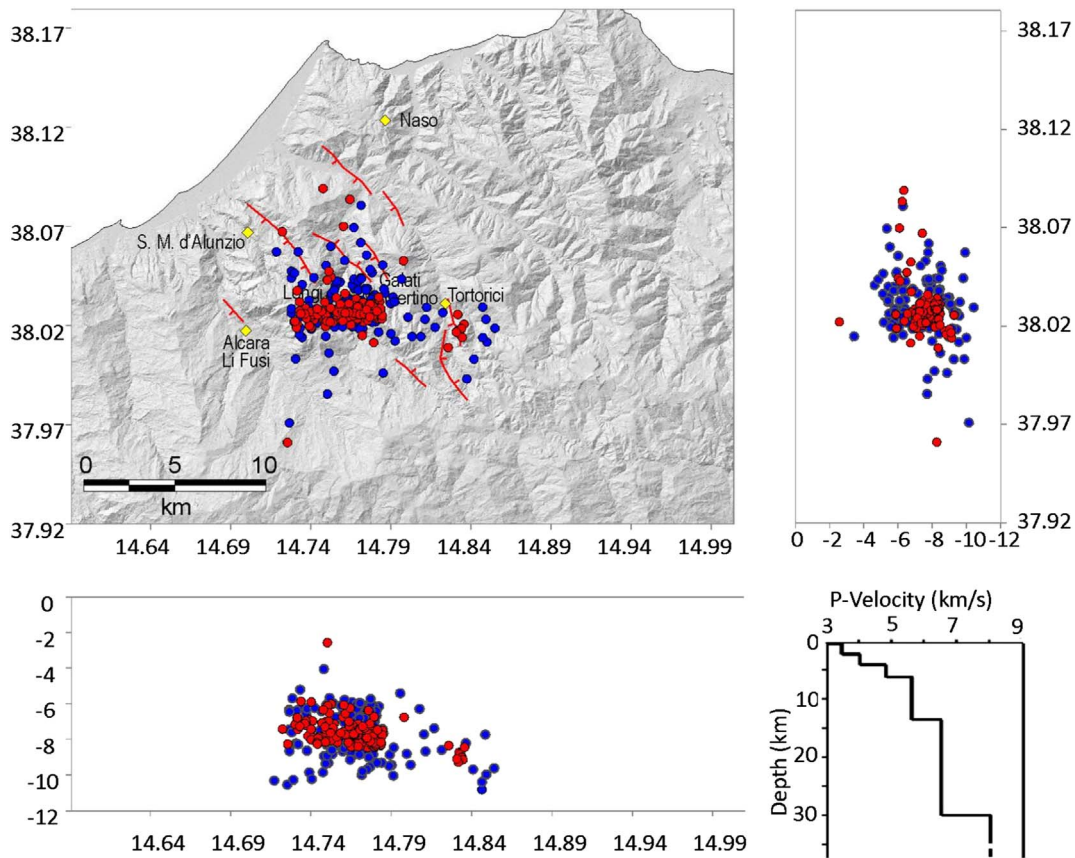


**Fig. 3.** Map and vertical cross-sections of the standard (blue circles) and relocated (red circles) seismicity. Active normal faults (barbed red line – barbs on downthrown block) are from Pavano et al. (2015) (modified). In the lower right panel the crustal 1D velocity model is reported (For interpretation of the references to colour in this figure legend, the reader is referred to the web version of this article.)

a magnitude of 4.6, with epicenter to the east of Galati Mamertino village at a depth of 7–8 km (red star in Fig. 2). The area most notably affected is located in a radius of 10 km from the epicenter, and including towns and municipalities such as: Tortorici, Galati Mamertino, Alcara li Fusi, Militello Rosmarino (Azzaro et al., 2014). The earthquake, felt by population, caused home fixtures to fall and, in some cases, even the furniture moved. In the historical centers of Tortorici, Galati Mamertino and Longi, minor damage also occurred in the masonry buildings (Azzaro et al., 2014). The main aftershocks were recorded on 27 June at 22:13 ( $M_L = 3.6$ ), 6 July at 9:08 ( $M_L = 4.0$ ) and 27 July at 04:03 ( $M_L = 3.5$ ). The depth of these events generally ranges between 5 and 10 km. Between 2012 and 2013, we recorded ~100 earthquakes in the same area; the strongest occurred on 1 April 2012 at 00:57 with  $M_L = 2.8$ , located ~2.3 km NW from Longi.

### 3.3. Data analysis

We computed accurate hypocenter locations (Fig. 3) by using the double-difference earthquake algorithm of Waldhauser and Ellsworth (2000) and the HypoDD routine (Waldhauser, 2001) on 130 events firstly located by using Hypoellipse (Lahr, 1989) and a local 1D velocity model derived from Hirn et al. (1991). The algorithm takes advantage of the fact that, if the hypocentral separation between two earthquakes is small enough with respect to both the event-station distance and the scale length of velocity heterogeneity, the ray paths are similar along almost the entire length (Got et al., 1994). Under this assumption, the differences in the travel times for two earthquakes recorded at the same station can be attributed to differences in their hypocenter spatial separation. In this way, errors due to inaccurately modeled velocity structure are minimized without needing station corrections.

HypoDD initially performed a reduction of the data because it groups the events into clusters of well-connected earthquakes and removes those considered outliers. In our analyses, all events are connected through a network of links consisting of 11424 P- and 2362 S-wave phase pairs. The average number of links per event pair was 16, while the average offset between strongly linked events was of about 1.74 km. New locations reduced standard errors showing mean hypocenter formal errors of ~300 m and ~330 m on the horizontal and vertical components, respectively. In the relocated catalogue, the mean RMS (Root Mean square) decreased from the initial value of 0.23 s to 0.11 s. As a result, we improved the quality of hypocenter locations with respect to the previously standard location performed in this study as well as the ones reported on on-line bulletins, which usually adopts regional-scale 1D velocity model (i.e., the Italian Seismological and Parametric database available at <http://iside.rm.ingv.it/iside/standard/index.jsp>). With respect to the standard locations, the relocated events show a more clustered disposition of hypocenters within a narrow range of depth, between 6 and 8.5 km, and distributed along a predominant E-W orientation (Fig. 3).

In order to define prospective time changes in repeating earthquakes, waveform similarities were quantitatively evaluated by adopting a cross-correlation coefficient (hereinafter referred to as CCC). Following Cannata et al. (2013), the CCC values were calculated to the whole dataset of the seismic swarm. In detail, the CCC analysis was computed by taking into account the waveforms recorded by the vertical component of MUCR station (Fig. 1), namely the station that recorded continuously throughout the period of interest and with greater energy. The signals were treated with a band-pass filter between 1 and 10 Hz. The correlations were made on time windows of 3 s (in order to include the whole phase P and the initial part of S), and starting from



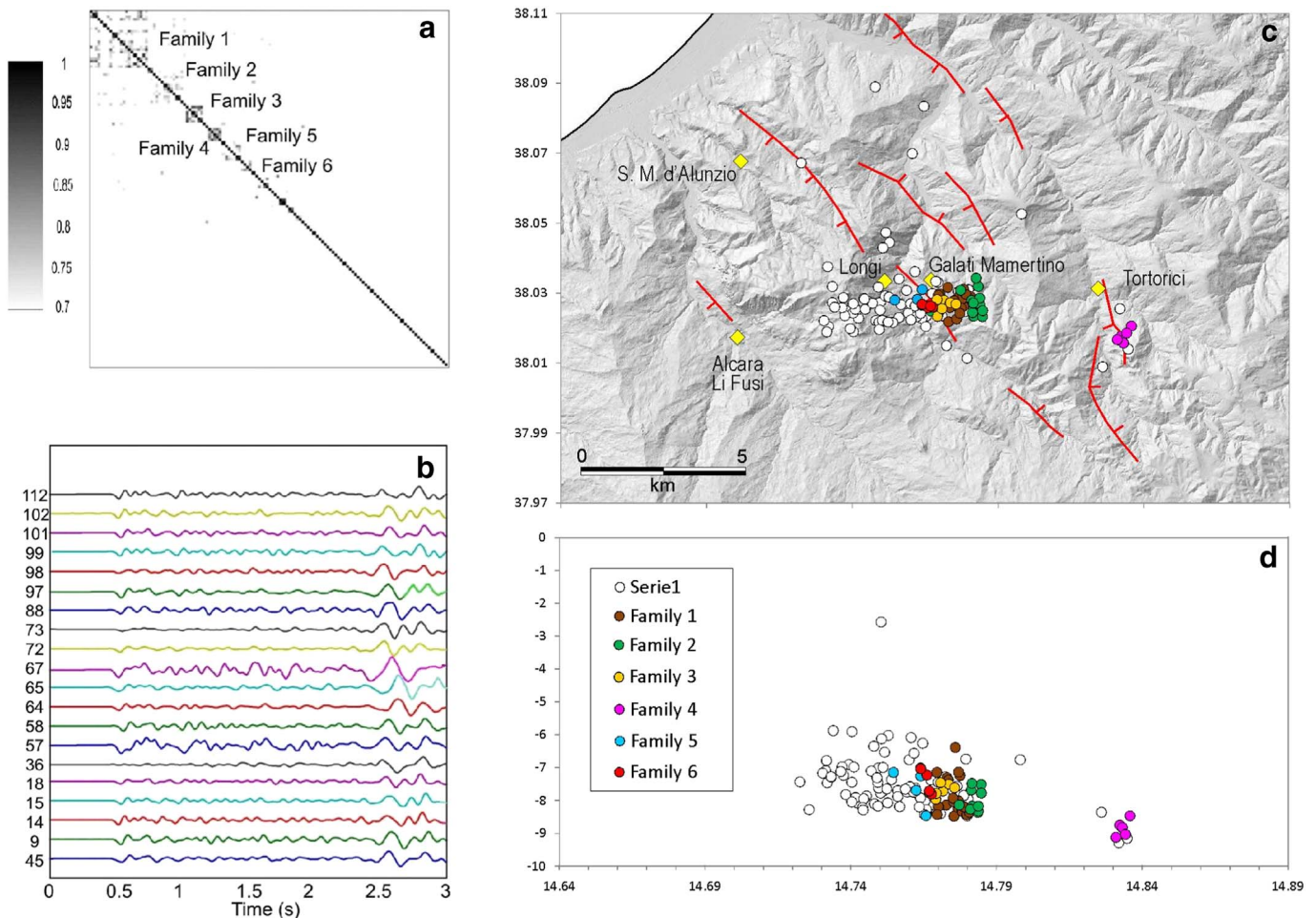


Fig. 4. Results of cross correlation: (a) the correlation matrix where the events with a correlation major of 0.7 are grouped in families; (b) example of seismic signals correlation related to family 1. (c) Map and (d) EW section of relocated events showing families position. White circles represent events out of families. Active normal faults (barbed red line – barbs on downthrown block) are from Pavano et al. (2015) (modified). (For interpretation of the references to colour in this figure legend, the reader is referred to the web version of this article.)

the P wave onset. Once obtained, the correlation matrix was analyzed by adopting the method of Green and Neuberg (2006) in order to extract the families of events characterized by similar waveforms. The correlation threshold was fixed at 0.7. Such analyses have shown that ~45% of the whole dataset is grouped in six families of seismic events (Fig. 4). The main feature coming from the CCC analysis is that events belonging to families are located in the eastern part of the seismogenetic volume while the western sector is characterized by earthquakes without similar waveforms.

Since this feature could reflect possible path effect at MUCR station, we performed an additional CCC analysis by considering the waveforms recorded at MNO station (positioned ~10 km SW from the cluster; see the Supplementary Material section for details). Such an additional analysis confirmed the existence of the families detected at MUCR and located in the eastern part of the seismogenetic volume. Moreover, it revealed the occurrence of some few couples of events with similar waveform also on the western part of the seismogenetic volume. All these observations highlighted the absence of path effects or that these effects can be considered negligible, therefore, lending credit to a difference in families clustering between the eastern and western side of the seismogenetic volume (see the Supplementary Material section for additional details).

We determined also the earthquake focal plane solutions (FPSs). They were obtained with the FPFIT code (Reasenber and Oppenheimer, 1985) by using the P-wave first motion polarity in vertical components. In detail, the FPFIT code searches the double-couple FPS that best fits the set of P-wave first motion polarities for an

earthquake. In some cases, FPFIT was unable to converge on a unique fault-plane solution, and instead returned two or more possible solutions. If multiple solutions for an earthquake were dissimilar (e.g. a normal solution and a strike-slip solution), they were rejected. When a unique solution, or similar multiple solutions, were obtained, the solutions were evaluated using the following criteria: i) number of polarities  $\geq 13$ , ii) number of polarity discrepancies  $< 3$ , iii) average uncertainty in strike, dip, and rake  $< 20^\circ$  and iv) pressure (P-) and tension (T-) axis regions that each covered  $< 25\%$  of the focal sphere. Fault-plane solutions that did not meet all of these criteria were rejected. Computed FPSs are reported in Table 1 and Fig. 5a. The Italian CMT catalogue (RCMT; <http://www.bo.ingv.it/RCMT/Italydataset.html>; Pondrelli et al., 2006) represents an extension toward smaller magnitudes of the Harvard Centroid Moment Tensor catalogue (<http://www.globalcmt.org>) and reports the FPSs, computed by using the waveform-inversion approach, for events occurred on 23 June and 6 July 2011, respectively (events n. 2 and n. 25 in Table 1). By comparing our solutions with those provided by RCMT as well as those reported in Presti et al. (2013) we observed very similar solutions, especially for the largest earthquake, hence in the following we refer to our solutions. FPSs show prevalently normal faulting features (95.5%), while remaining solutions are characterized by strike-slip or oblique normal faulting features (Fig. 5a). Moreover, the distribution of P- and T- axes reveals that the former are prevailing subvertical, while the latter show a large scatter with a prevailing concentration along the NNW-SSE orientation.

FPSs were inverted to determine the principal stress axes

**Table 1**FPSs computed in this study. Date is in format day-month-year; O.T. = origin time (hour and minute); latitude north and longitude east; depth in km;  $M_L$  = local magnitude.

| N  | Date       | O.T.  | Lat. (°E) | Lon. (°N) | $M_L$ | Depth (km) | Strike (°) | Dip (°) | Rake (°) | Family |
|----|------------|-------|-----------|-----------|-------|------------|------------|---------|----------|--------|
| 1  | 11/06/2011 | 15:15 | 38.0089   | 14.8259   | 2.2   | 8.36       | 75         | 40      | −70      |        |
| 2  | 23/06/2011 | 22:02 | 38.0331   | 14.7693   | 4.6   | 8.39       | 65         | 45      | −130     |        |
| 3  | 24/06/2011 | 00:46 | 38.0343   | 14.7824   | 2.7   | 8.29       | 50         | 60      | −120     | 2      |
| 4  | 24/06/2011 | 04:08 | 38.0234   | 14.7653   | 2.6   | 8.03       | 35         | 40      | −130     |        |
| 5  | 24/06/2011 | 14:37 | 38.0444   | 14.7527   | 2.8   | 6.03       | 260        | 70      | −60      |        |
| 6  | 24/06/2011 | 17:57 | 38.0267   | 14.7835   | 2.7   | 8.36       | 50         | 35      | −120     | 2      |
| 7  | 25/06/2011 | 18:35 | 38.0292   | 14.7512   | 2.6   | 7.70       | 50         | 45      | −120     |        |
| 8  | 26/06/2011 | 01:18 | 38.0243   | 14.7592   | 2.5   | 7.75       | 130        | 35      | −80      |        |
| 9  | 26/06/2011 | 02:37 | 38.0261   | 14.7657   | 1.8   | 8.46       | 75         | 75      | −70      | 5      |
| 10 | 27/06/2011 | 05:23 | 38.0228   | 14.7421   | 3.3   | 8.07       | 40         | 65      | −120     |        |
| 11 | 27/06/2011 | 07:15 | 38.0288   | 14.7525   | 2.7   | 8.07       | 100        | 25      | −110     |        |
| 12 | 27/06/2011 | 17:42 | 38.0204   | 14.7652   | 2.7   | 8.43       | 20         | 30      | −140     |        |
| 13 | 27/06/2011 | 22:13 | 38.0250   | 14.7382   | 3.6   | 7.83       | 40         | 60      | −120     |        |
| 14 | 28/06/2011 | 00:43 | 38.0221   | 14.7481   | 2.6   | 8.10       | 5          | 55      | −110     |        |
| 15 | 28/06/2011 | 08:25 | 38.0263   | 14.7753   | 3.0   | 8.48       | 60         | 50      | −100     | 1      |
| 16 | 28/06/2011 | 11:54 | 38.0242   | 14.7634   | 2.9   | 8.19       | 45         | 50      | −120     |        |
| 17 | 29/06/2011 | 09:04 | 38.0243   | 14.7402   | 3.2   | 8.04       | 135        | 35      | −80      |        |
| 18 | 29/06/2011 | 19:15 | 38.0276   | 14.7453   | 3.3   | 7.87       | 105        | 75      | −140     |        |
| 19 | 30/06/2011 | 09:49 | 38.0269   | 14.7403   | 2.7   | 7.45       | 55         | 45      | −140     |        |
| 20 | 30/06/2011 | 14:32 | 38.0340   | 14.7560   | 2.4   | 7.88       | 40         | 40      | −130     |        |
| 21 | 30/06/2011 | 21:02 | 38.0221   | 14.7501   | 2.9   | 7.78       | 40         | 45      | −100     |        |
| 22 | 02/07/2011 | 19:33 | 38.0235   | 14.7706   | 2.7   | 8.40       | 35         | 55      | −80      |        |
| 23 | 04/07/2011 | 09:36 | 38.0316   | 14.7727   | 3.3   | 8.14       | 45         | 60      | −100     | 1      |
| 24 | 05/07/2011 | 14:46 | 38.0279   | 14.7715   | 2.5   | 7.71       | 115        | 45      | −90      | 3      |
| 25 | 06/07/2011 | 09:08 | 38.0309   | 14.7798   | 4.0   | 8.47       | 40         | 55      | −110     |        |
| 26 | 06/07/2011 | 09:52 | 38.0361   | 14.7614   | 2.6   | 7.75       | 35         | 70      | −120     |        |
| 27 | 06/07/2011 | 15:56 | 38.0294   | 14.7694   | 2.5   | 8.43       | 35         | 60      | −110     | 1      |
| 28 | 06/07/2011 | 23:58 | 38.0233   | 14.7692   | 2.4   | 7.79       | 165        | 35      | −70      | 3      |
| 29 | 07/07/2011 | 01:01 | 38.0311   | 14.7781   | 3.2   | 8.34       | 40         | 70      | −90      | 1      |
| 30 | 08/07/2011 | 13:11 | 38.0272   | 14.7735   | 2.4   | 7.50       | 155        | 30      | −50      | 3      |
| 31 | 09/07/2011 | 19:05 | 38.0291   | 14.7797   | 2.7   | 8.43       | 50         | 40      | −110     | 1      |
| 32 | 09/07/2011 | 19:05 | 38.0290   | 14.7806   | 2.9   | 8.36       | 40         | 45      | −120     | 1      |
| 33 | 10/07/2011 | 06:14 | 38.0279   | 14.7809   | 2.3   | 8.27       | 70         | 40      | −130     | 2      |
| 34 | 11/07/2011 | 01:16 | 38.0260   | 14.7676   | 2.6   | 7.81       | −40        | 60      | −100     | 6      |
| 35 | 11/07/2011 | 04:49 | 38.0375   | 14.7316   | 1.8   | 6.79       | 85         | 45      | −70      |        |
| 36 | 15/07/2011 | 13:43 | 38.0310   | 14.7639   | 1.6   | 7.26       | 60         | 50      | −100     | 5      |
| 37 | 23/07/2011 | 06:14 | 38.0247   | 14.7787   | 2.8   | 7.85       | 55         | 55      | −130     |        |
| 38 | 23/07/2011 | 09:02 | 38.0526   | 14.7980   | 2.0   | 6.77       | 105        | 70      | −70      |        |
| 39 | 27/07/2011 | 04:03 | 38.0262   | 14.7668   | 3.5   | 7.72       | 150        | 30      | −80      | 6      |
| 40 | 07/08/2011 | 21:50 | 38.0284   | 14.7777   | 2.4   | 8.16       | 40         | 55      | −110     | 1      |
| 41 | 25/08/2011 | 13:07 | 38.0286   | 14.7837   | 2.4   | 8.18       | 70         | 25      | −140     | 2      |
| 42 | 31/03/2012 | 13:09 | 38.0285   | 14.7439   | 2.4   | 8.21       | −10        | 55      | −130     |        |
| 43 | 01/04/2012 | 00:57 | 38.0283   | 14.7441   | 2.8   | 8.29       | 15         | 60      | −90      |        |
| 44 | 04/09/2013 | 09:23 | 38.0185   | 14.8341   | 2.1   | 9.03       | 95         | 45      | −20      | 4      |
| 45 | 06/09/2013 | 19:39 | 38.0167   | 14.8309   | 1.6   | 9.12       | 165        | 35      | −160     | 4      |

$\sigma_1 \geq \sigma_2 \geq \sigma_3$  and the dimensionless stress ratio  $R$  ( $\sigma_1 - \sigma_2 / \sigma_1 - \sigma_3$ ) by using an iterative approach (Vavryčuk, 2014), where in each iteration the stress field orientation is calculated and the fault plane with higher instability coefficient (out of the two possible in a focal mechanism) is selected for the next inversion iteration. Such an instability coefficient quantifies how close a fault is to an optimal orientation given a stress state and a friction coefficient (Vavryčuk, 2014). In order to avoid the sensitivity of the inversion to friction, needed in the instability constraint, the inversion was run repeatedly with friction ranging from 0.05 to 1 in steps of 0.05. For each friction, an overall instability of faults identified by the inversion was evaluated, and the friction, which produced the highest overall fault instability, was considered as optimum. In order to evaluate possible changes in the stress field, we performed different inversions by grouping the events in two main sub-datasets (namely Group A and Group B). We defined the two datasets by taking into account their CCC values, as estimated for MUCR station since we observed that events characterized by similar waveforms are mainly located in the eastern part of the seismogenetic area (Group A), while in the western part (Group B), with the exception of few couples of events, the remaining events show no similar waveforms. Moreover, we performed an inversion by taking into account the whole dataset; obtained results are reported in Fig. 5b and Table 2. All the resulting stress tensors are characterized by a nearly vertical  $\sigma_1$  and sub-

horizontal  $\sigma_2$  and  $\sigma_3$ , this last showing a NW-SE attitude. The shape ratio  $R$  and optimum friction shows values of  $\sim 0.8$  and  $\sim 0.4$ , respectively. These results clearly indicate that, beside the slight difference in friction coefficient values (0.40 and 0.35 for group A and B, respectively), there are no significant differences in terms of stress field orientation and shape between groups A and B, hence in the following we refer to results achieved by inverting the whole dataset.

#### 4. Structural analysis

We performed a detailed field surveys data acquisition about mesoscale fault geometries and kinematics in the area affected by the 2011 seismic swarm (localized between Galati Mamertino and Longi villages; Fig. 2) in order to detect Holocene expressions of faulting activity. To this end, we collected > 300 structural measurements, distributed on 13 measure stations (Fig. 2) located within a narrow belt including the main rejuvenated NW-SE oriented normal fault segments affecting the seismogenetic volume (see also SGL - San Marco d'Alunzio-Galati Line in Pavano et al., 2015). We utilized structural data to obtain an inversion of the stress tensors from the fault kinematics. We pursued this goal by measurements that were exclusively performed on tectonic features on the Liassic limestone, avoiding collecting data on the Hercynian epimetamorphic basement, in order to filter any structure

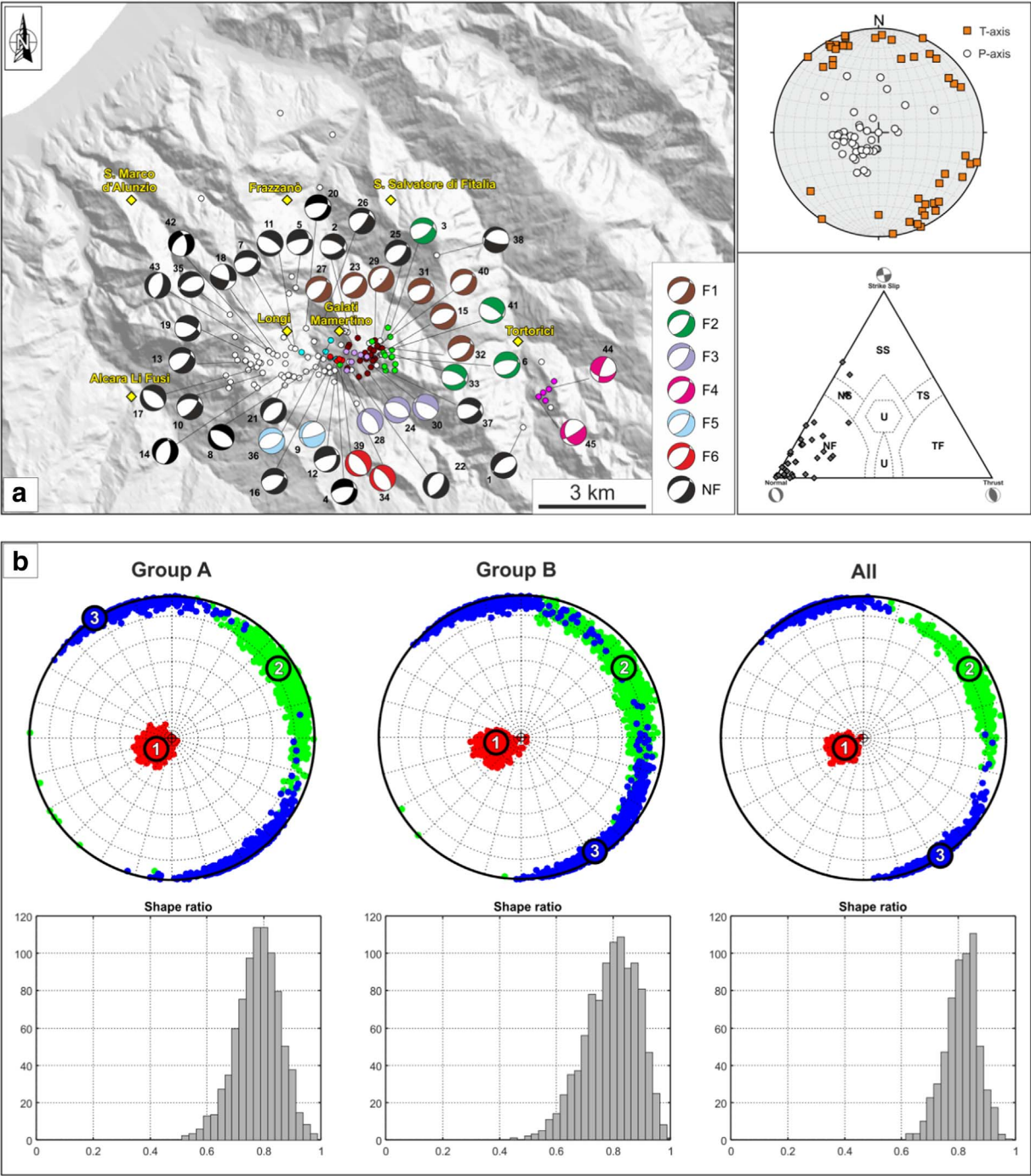


**Fig. 5.** (a) Map of the investigated area with fault plane solutions computed in this study. FPSs are colored according to the family events (see Table 1 for numbers and additional details). Right-hand panels show the P- and T-axes distribution on equal-area lower hemisphere projection (upper panel) and a ternary plot of FPSs (lower panel). Each point is plotted based on the plunge of the P-, T- and B-axes of the mechanism (Frohlich, 1992). The dashed line divides the triangle into faulting styles based on definitions by Zoback (1992): NF is normal faulting, NS is normal and strike-slip, SS is strike-slip, TS is thrust and strike-slip, TF is thrust faulting and U is undefined. (b) Stress tensor inversion results for groups A, B and All (see the main text for details) reported as confidence limits of each principal stress directions and the dimensionless stress ratio R.

**Table 2**  
Results of stress inversions. The errors are the maximum differences between the results calculated for the noise-free and noisy focal mechanisms with 1000 random realizations (see Vavryčuk, 2014 for additional details).

|     | N° FPS | $\sigma_1$ Az./pl. | $\sigma_2$ Az./pl. | $\sigma_3$ Az./pl. | R          | Friction |
|-----|--------|--------------------|--------------------|--------------------|------------|----------|
| A   | 24     | 236°/79° ± 15°     | 57°/11° ± 68°      | 327°/0° ± 68°      | 0.78 ± 40% | 0.40     |
| B   | 21     | 257°/75° ± 17°     | 56°/14° ± 88°      | 147°/5° ± 88°      | 0.83 ± 50% | 0.35     |
| All | 45     | 245°/78° ± 12°     | 56°/12° ± 59°      | 147°/2° ± 59°      | 0.84 ± 31% | 0.40     |



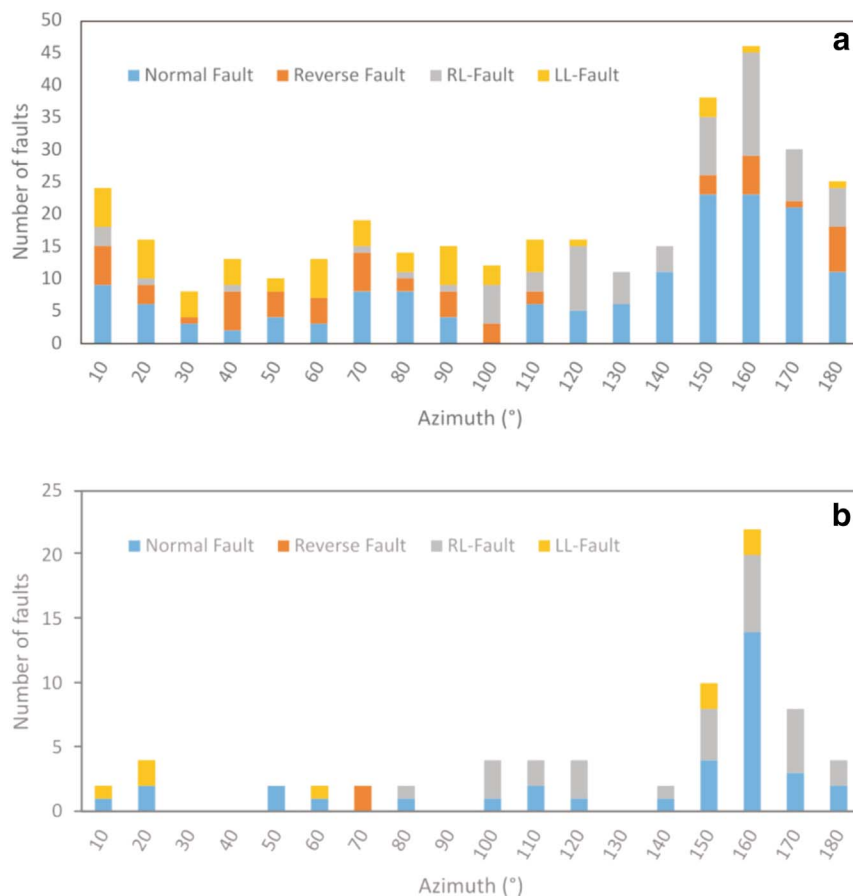


**Fig. 6.** a) Azimuthal distribution of the entire dataset of shear planes distinguished by kinematic; b) Azimuthal distribution of the selected shear planes showing two generations of striae, distinguished by kinematic.

related to both older dynamics and metamorphism processes of the crystalline units.

On-field collected data, grouped by both azimuth and kinematics, show a well-confined distribution, especially as regards the normal faults and the right-lateral strike slip faults (Fig. 6a). Normal faults are mainly distributed between N140° and N180°, showing a maximum around N150°–170° and minor distributions at N10° and N70°–80° (Fig. 6a). The right-lateral strike-slip faults show a similar azimuthal distribution, strongly clustering around N150°–160° and less so around N120° and N170°–180° (Fig. 6a). Conversely, both reverse and left-lateral strike-slip fault have a sparse azimuthal distribution. Reverse faults cluster between N40° and N70°, with minor groups at N10°, N160° and N180° (Fig. 6a). The left-lateral strike-slip faults are extremely spread out in the N10° and N110°, without a relevant clustering, and no significant data falling between N120° and N180° (Fig. 6a). Considering only the fault planes showing more than one generation of kinematic indicators (Fig. 6b and Table 3), a clear poly-phase tectonic picture arises. In these cases, the stress tensors were obtained by inversion of the last two overlapped slickensides, neglecting, where recognised, the older ones, generally sparse and not significant. We processed separately data obtained by mesoscale measurements carried out in the footwall and in the hangingwall of the principal fault segments.

The selected fault planes show an overlapped azimuthal distribution of younger normal faults (Pitch = 90°) on previous dextral faults (Pitch = 15° and 160°) mainly around both N150°–170° and N100°–120° (Fig. 6b), whereas few faults display left-lateral strike-slip motions (Pitch = 25° and 160°) replaced by pure extensional movements at N10°–20° and N150°–160° (Fig. 6b). These distributions are consistent with the results obtained considering the entire data record (Fig. 6a), assuming that the one-kinematic shear planes are indicative of either more recent or older movements. In conclusion, we recognise

two distinct, coherent structural and kinematic arrays. The oldest of the two is composed of main NW-SE oriented right-lateral faults (Pitch = 150°–180°), together with NNW-SSE and ESE-WNW oriented right-lateral strike-slip faults, minor NE-SW oriented left-lateral strike slip faults (Pitch = 15° and 165°) and NE-SW to ENE-WSW trending reverse faults (Pitch = 85°–90°). This arrangement reproduces the Riedel shear fault pattern linked to the deformation along the main NW-SE oriented right-lateral strike-slip faults and their subsidiary faults, such as the synthetic P and R shears and the antithetic P' and R'.

The main right-lateral strike-slip faults, including P and R shears, as well as the subordinate P' and R' shears (left-lateral faults), have been rejuvenated as normal faults (Pitch = 80°–100°) (Fig. 6b). These inferences are also supported by the good overlapping of the azimuthal distribution of these two groups of faults.

The fault-slip analysis results in two similar couples of moment tensor solution (Fig. 7). Like those obtained for the footwall (Fig. 7a–b), the hangingwall (Fig. 7c–d) shear planes concur with an earlier dextral kinematic with  $\sigma_1$  oriented about NNE-SSW with a WNW-ESE oriented  $\sigma_3$  (Fig. 7a and c), whereas the youngest kinematic responds to a main NE-SW extension, with an almost vertical  $\sigma_1$  (Fig. 7b and d). Overall, we did not recognise pronounced differences between the two structural domains, suggesting a uniform response to the most recent extensional dynamics, characterized by homogeneous kinematic and structural paths.

## 5. Discussion

We analyzed a seismic swarm (> 2700 events with local magnitude  $M_L \geq 1.3$ ) striking the Nebrodi Mountains (north-eastern Sicily) during June 2001–September 2013. The highest magnitude reached  $M_L = 4.6$ , and focal depths ranged from 5 to 9 km, with an average depth of 7–8.5 km. In the regional seismotectonic framework, the seismogenetic



**Table 3**

Selected shear planes showing two groups of slickensides, with clear kinematics over-lapping. The data gained on the footwall and hangingwall block are distinguished.

| Measure st. | Azimuth<br>(RHR) (°) | Dip (°) | Pitch 1 (°) | Kin. 1 (°) | Pitch 2 (°) | Kin. 2 (°) |
|-------------|----------------------|---------|-------------|------------|-------------|------------|
| FOOTWALL    |                      |         |             |            |             |            |
| S1          | 10                   | 85 E    | 20          | Sx         | 50          | N          |
| S2          | 110                  | 70 N    | 0           | Dx         | 120         | N          |
| S2          | 105                  | 50 N    | 5           | Dx         | 100         | N          |
| S2          | 100                  | 50 N    | 0           | Dx         | 20          | Dx         |
| S2          | 160                  | 70 E    | 25          | Dx         | 100         | N          |
| S3          | 165                  | 80 W    | 170         | Dx         | 25          | Dx         |
| S3          | 175                  | 75 E    | 5           | Dx         | 90          | N          |
| S3          | 150                  | 80 E    | 130         | Sx         | 30          | Sx         |
| S3          | 160                  | 70 E    | 0           | Dx         | 165         | Sx         |
| HANGINGWALL |                      |         |             |            |             |            |
| S4          | 20                   | 80 W    | 30          | Sx         | 60          | N          |
| S4          | 135                  | 80 SW   | 170         | Dx         | 135         | N          |
| S5          | 160                  | 70 E    | 50          | Dx         | 100         | N          |
| S5          | 160                  | 60 E    | 50          | Dx         | 100         | N          |
| S5          | 150                  | 60 NE   | 45          | Dx         | 100         | N          |
| S5          | 100                  | 85 N    | 10          | Dx         | 60          | N          |
| S6          | 60                   | 70 SE   | 20          | Sx         | 50          | N          |
| S6          | 150                  | 60 NE   | 5           | Dx         | 140         | Dx         |
| S7          | 155                  | 30 E    | 100         | N          | 85          | N          |
| S8          | 160                  | 30 E    | 115         | N          | 160         | Sx         |
| S8          | 160                  | 70 E    | 120         | N          | 70          | N          |
| S9          | 65                   | 80 SE   | 80          | I          | 100         | I          |
| S9          | 150                  | 80 NE   | 0           | Dx         | 50          | N          |
| S9          | 120                  | 60 SW   | 20          | Dx         | 150         | Dx         |
| S10         | 80                   | 60 S    | 170         | Dx         | 100         | N          |
| S11         | 160                  | 60 E    | 95          | N          | 110         | N          |
| S11         | 20                   | 75 E    | 15          | Sx         | 70          | N          |
| S11         | 120                  | 60 NE   | 160         | Dx         | 60          | N          |
| S11         | 0                    | 80 E    | 10          | Dx         | 70          | N          |
| S11         | 175                  | 75 E    | 0           | Dx         | 130         | N          |
| S11         | 155                  | 80 NE   | 0           | Dx         | 90          | N          |
| S11         | 160                  | 75 E    | 5           | Dx         | 60          | N          |
| S11         | 165                  | 85 E    | 0           | Dx         | 65          | N          |
| S12         | 170                  | 70 W    | 5           | Dx         | 100         | N          |
| S12         | 165                  | 75 W    | 5           | Dx         | 95          | N          |
| S12         | 150                  | 85 SW   | 110         | N          | 100         | N          |
| S12         | 155                  | 80 W    | 130         | N          | 100         | N          |
| S12         | 45                   | 60 NW   | 70          | N          | 100         | N          |
| S12         | 0                    | 60 W    | 130         | N          | 80          | N          |

volume is located at the southern edge of the Calabrian arc (Chiarabba and Palano, 2017). The earthquake swarm sequence defines an E-W oriented seismogenetic area, which does not correspond to the azimuthal distribution (mainly clustering around N150°–180°E) of fault segments and tectonic features mapped on field (Fig. 2) (Pavano et al., 2015).

Results coming from CCC analysis on MUCR and MNO stations highlighted the existence of at least six families of multiplet seismic events that are exclusively located in the eastern part of the seismogenetic volume, while such a main feature is less evident on the western sector (Fig. 4). Such a difference in the occurrence of multiplet events would suggest a different mechanical behavior between the western and eastern sector of the seismogenetic volume. However, this difference seems not depending from frictional parameters alone, since analysis performed in this study inferred a not relevant difference in friction coefficient values (0.40 and 0.35 for eastern and western sector of the seismogenetic group, respectively).

At the surface, the seismogenetic volume encompasses the tectonic boundary between the Hercynian crystalline units of the Calabrian arc, extensively outcropping in the north-eastern sector of the investigated area (Fig. 2) and the accretionary wedge terrains of the Sicilide units, outcropping in the south-western sector of the study area. At a depth of 10 km, at which the 2011–2013 seismic swarm events are confined, such a boundary is highlighted by the seismic velocity tomography as a sharp transitional zone between a north-eastern high-velocity domain

and a south-western low-velocity one (Palano et al., 2015). In such a context, the occurrence of multiplet seismic events is favored in the high-grade metamorphic rocks basement, while the accretionary wedge terrains do not allow the repeating rupture of the same fault patch, implying that the distinguished families of multiplet seismic events would be responsive to the lateral variations in lithology (hence in mineralogical composition, density, elastic parameters, etc.) at depth (Fig. 8). The mechanisms causing multiplet events are not completely understood; however, a number of studies have highlighted that the occurrence of persistent seismic activity can also be related to changes in pore fluid pressure that may reduce crustal strength and promote fault slip (see Miller et al., 2004 for an overview). The hypothesis is that an increase in fluid pressure reduces the effective normal stress, effectively weakening the fault and shear strength to a level below the prevailing shear stress. Camarda et al. (2016), by analyzing soil CO<sub>2</sub> flux measurements collected by a local network over north-eastern Sicily, observed a clear spatial and temporal correlation between seismicity and gas discharge. This fact highlights the widespread occurrence of over-pressured fluid emissions at the surface over the investigated area as focused and/or diffuse gas emissions often associated with thermal fluids, therefore evidencing the migration of mantle fluids toward the surface along lithospheric pathways (e.g. faults). In light of this, we suggest that the seismic swarms striking the investigated area can be triggered by pore pressure transients due to mantle fluid flows.

Computed FPSs show prevalently normal faulting features (95.5%) with T axes showing a large scatter with a prevailing concentration along the NNW-SSE orientation. FPSs were inverted to determine the principal stress axes  $\sigma_1 \geq \sigma_2 \geq \sigma_3$  and the dimensionless stress ratio R ( $\sigma_1 - \sigma_2 / \sigma_1 - \sigma_3$ ). The resulting stress tensor is characterized by a nearly vertical  $\sigma_1$  and sub-horizontal  $\sigma_2$  and  $\sigma_3$ , this last showing a NW-SE attitude (Fig. 5). This result, coupled with a stress ratio R value of  $\sim 0.8$ , clearly indicates a nearly biaxial stress state in an extensional regime with  $\sigma_1 > \sigma_2 \cong \sigma_3$ , such that crustal extension occurs along the NW-SE and along the NE-SW directions. Such a feature matches well with geological data which, by detailed field surveys, allowed us to recognise two distinct structural and kinematic arrays. The oldest is composed of main NW-SE oriented right-lateral faults, coupled with secondary faults organized into a NNW-SSE, ESE-WNW and NE-SW to ENE-WSW arrangement. This arrangement can be related with to the progressive ESE-ward migration of the Calabrian arc that, during the Plio-Pleistocene, was accommodated by the development of a wider W-E trending lithospheric right-lateral shear zone, characterized by both NW-SE/W-E dextral faults oriented and left-lateral N-S/NE-SW fault arrays (Finetti et al., 1996; Giunta et al., 2009). The development of these fault arrays corresponds to a spatial and temporal progression from active subduction to slab detachment and recently, to the onset of compression confined along the northern Sicilian off-shore (see Chiarabba and Palano, 2017 and reference therein). Such a pre-fractured crustal domain has been involved, according to different kinematics, in a coherent and more recent dynamic. This latter, which replaces the previous one, cause a reorientation of stress axes, from horizontal, NNW-SSE trending, to vertical, leading to diffuse extensional processes and the inversion of the strike-slip faults as normal faults, implying a negative reactivation of the previous Riedel shear fault configuration. This more recent kinematic is the expression of the crustal response to the tectonic uplift that involved the north-eastern Sicily crustal domain from the Middle Pleistocene (600 ka) (Catalano and Di Stefano, 1997; Pavano et al., 2015), resulting in the fragmentation of the southern termination of the Calabrian Arc (Catalano et al., 2008; Pavano et al., 2016). Nevertheless, although the inversion of the collected mesoscale fault planes points to a prevailing NE-SW oriented extension (Fig. 7), actually, a radial dispersion of the resulting kinematic vectors arises, in accordance with the FPSs inversion data. These results support the idea of mantle upwelling processes, which would occur beneath the studied region, where, at depth, sub-crustal over-

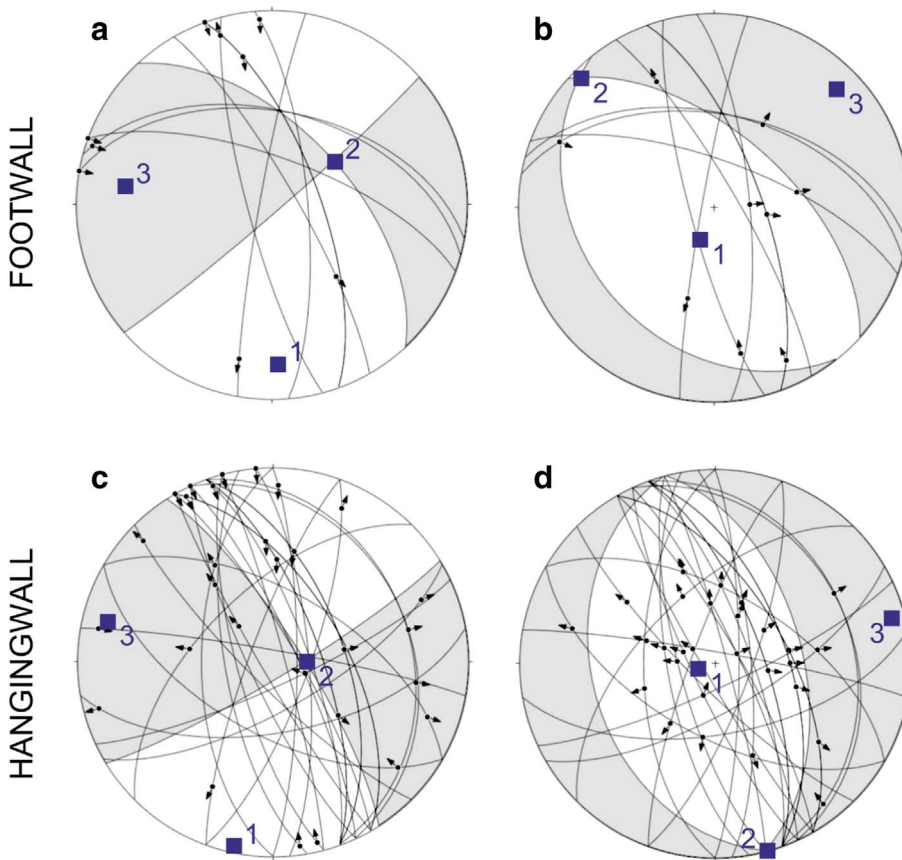


Fig. 7. Stress tensor solutions resulting by fault inversion analysis of shear planes: (a) plot results from older and (b) the youngest kinematics obtained from the data falling within the footwall; (c) plot results from older and (d) the youngest kinematics from data falling within the hanging-wall. Black dots indicate the rake values and black arrows the direction and the sense of movement. Blue squares represent the main axes of stress: 1 =  $\sigma_1$ ; 2 =  $\sigma_2$ ; 3 =  $\sigma_3$ . (For interpretation of the references to colour in this figure legend, the reader is referred to the web version of this article.)

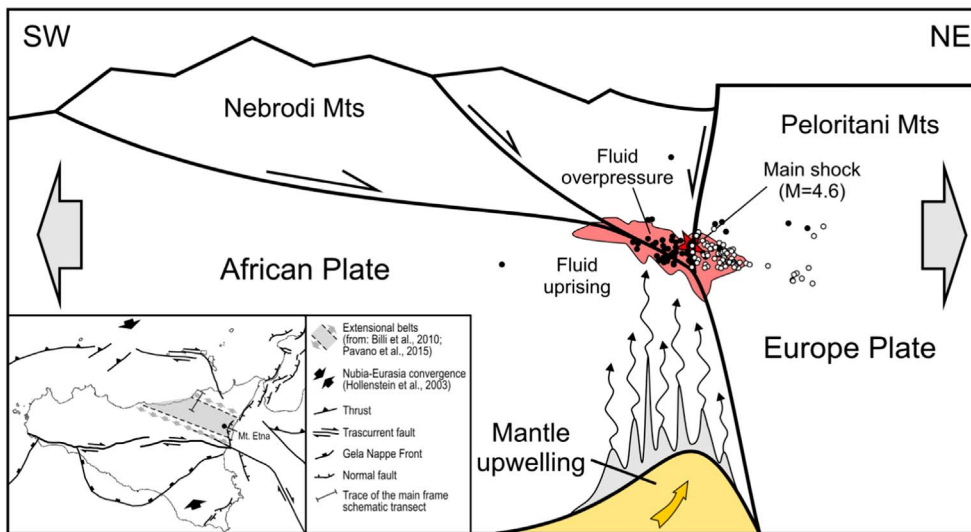


Fig. 8. Schematic transect across the boundary between Nebrodi Mts. and Peloritani Mts., at the southern termination of the Calabrian, where diffuse normal faulting along previous thrust and high-angle strike-slip faults occurs. Mantle upwelling, fluid migration and fluid overpressure region at depth, invoked to model our results, are sketched. The seismic events belonging to both the Group A (white circles) and the Group B (black circles) and the 4.6 main shock (red star) are reported. The inset map shows a simplified interpretative model for north-eastern Sicily in the frame of the regional scale tectonic and kinematic context. (For interpretation of the references to colour in this figure legend, the reader is referred to the web version of this article.)

pressured fluids migrate toward the surface by exploiting the crustal dense network of faults and fractures.

Moreover, the investigated area, localized at the westward tapering of the regional uplift pattern of the Calabrian arc (Ferranti et al., 2010; Faccenna et al., 2011), can be framed in a wider (~20–30 km) NW-SE-oriented extensional belt. This latter would include the Madonie-Mt. Etna volcano alignment, characterized by crustal stretching along both the NW-SE, N-S and the NE-SW directions, as testified by previous seismological (Neri et al., 2006; Presti et al., 2013; Orecchio et al., 2017), geodetic (Palano et al., 2015; Chiarabba and Palano, 2017) and geological (Billi et al., 2010) observations.

Several authors have explained the occurrence of these crustal

stretching processes, mainly framed within a prevalent compressive domain, by resorting to different mechanisms, even if this topic is still an open question in recent scientific debate. Lavecchia et al. (2007) view this crustal stretching as ensuing from upper crustal stretching above an active thrust belt, while Billi et al. (2010) and Pavano et al. (2012, 2015) point to the reactivation of pre-existing faults and mantle upwelling.

In this regards, from a tectonic-kinematic point of view, such a wider NW-SE-oriented extensional belt (Billi et al., 2010; Pavano et al., 2015) is located at the eastern termination of a compressional belt confined between the locked front of the Maghrebien Apennines (i.e. Gela Nappe; Lickorich et al., 1999), except for the north-eastern margin

of the Hyblean Plateau (Musumeci et al., 2014; Bonforte et al., 2015; Chiarabba and Palano, 2017), and the resumed south Tyrrhenian compressional belt (Billi et al., 2007, 2011) (Fig. 8). In the context of the Ionian subduction zone, a main role was played by the progressive eastward slab rollback leading therefore to i) the detachment of the Ionian lithosphere beneath the northern margin of Sicily (see Chiarabba and Palano, 2017), ii) the opening of a mantle window along the south-eastern edge of the slab (Gvirtzman and Nur, 1999; Doglioni et al., 2001) and iii) the upwelling of asthenospheric material (e.g. Trua et al., 2003). In this regards, as a whole, we suggest a strictly relation between the asthenospheric material upwelling and the extensional dynamics of the region, as well as the high-rate tectonic uplift (1.1 mm/yr; Catalano and Cinque, 1995; Catalano and Di Stefano, 1997; Pavano et al., 2015) and the occurrence of diffuse gas emissions (Camarda et al., 2016) (Fig. 8).

In such a context, the Nubia-Eurasia NNW-SSE-trending convergence (Hollenstein et al., 2003; Goes et al., 2004) is primarily accommodated in the Tyrrhenian offshore. A fraction of such convergence is still accommodated along the north-eastern margin of the Hyblean Plateau and would be also presently accommodated by a E-W-oriented right-lateral strike-slip deformation in central Sicily as suggest by Gueguen et al., 2002, Catalano et al., 2008; Catalano et al., 2017b (Fig. 8).

## 6. Conclusive remarks

Seismic and geological data presented in this study help improve the picture of the seismogenetic pattern at the southern edge of the Calabrian arc.

We analyzed a seismic swarm sequence occurring in the Nebrodi Mts. area during 2011–2013, in the 5–9 km depth interval. Such a seismic swarm defined an E-W oriented seismogenetic volume encompassing the NW-SE tectonic boundary between the Hercynian crystalline units of the Calabrian arc (north-eastward) and the accretionary wedge terrains of the Sicilide units (south-westward).

By analyzing the entire seismic dataset, we observed that earthquakes showing similar waveforms are located only on the eastern part of the seismogenetic volume, evidencing the responsivity to changes in lithology at depth. Structural analysis evidences that the structural path of the investigated area, after an early stage dominated by dextral strike-slip faulting, underwent a reactivation of the same Riedel shear planes path under an extensional dynamic. Stress tensor inversions performed on FPSs and fault slip data indicate that the investigated area is currently subject to a nearly biaxial stress state in an extensional regime, such that crustal extension occurs along both NW-SE and NE-SW directions.

This prevailing extension can be related to a mantle upwelling process (as evidenced by the presence of diffuse mantle-derived gas emissions) coupled with a tectonic uplift involving north-eastern Sicily since the Middle Pleistocene. Thus, the seismic swarms striking the Nebrodi Mountains would be related to the mantle upwelling and the migration of sub-crustal over-pressured fluids toward the surface along the complex network of tectonic structures that cut the crust and act as pathways.

## Acknowledgements

We are indebted to the technicians of the INGV who ensured the regular working of the seismic network. We thank the Editor in chief Keli Wang, Andrea Billi and an anonymous referee for their useful comments and suggestions, which helped us to improve significantly the early version of paper.

## Appendix A. Supplementary data

Supplementary data to this article can be found online at <https://doi.org/10.1016/j.tecto.2017.11.021>.

[doi.org/10.1016/j.tecto.2017.11.021](https://doi.org/10.1016/j.tecto.2017.11.021).

## References

- Alparone, S., Gambino, S., 2003. High precision locations of multiplets on south-eastern flank of Mt. Etna (Italy): reconstruction of fault plan geometry. *Phys. Earth Planet. Inter.* 135, 281–289.
- Amodio-Morelli, L., Bonari, G., Colonna, V., Dietrich, D., Giunta, G., Ippolito, F., Liguori, V., Lorenzoni, S., Paglionico, A., Perrone, V., Piccarreta, G., Russo, M., Scandone, P., Zanettin-Lorenzoni, E., Zappetta, A., 1976. L'Arco Calabro-peloritano nell'orogene appenninico-maghrebide. *Mem. Soc. Geol. Ital.* 17, 1–60.
- Anderson, H.A., Jackson, J.A., 1987. The deep seismicity of the Tyrrhenian Sea. *Geophys. J. R. Astron. Soc.* 91, 613–637.
- Azzaro, R., D'Amico, S., Mostaccio, A., Scarfi, L., Tuvè, T., Manni, M., 2014. Terremoti con effetti macrosismici in Sicilia orientale nel periodo Gennaio 2009–Dicembre 2013. *Quad. Geofis.* 120 (ISSN 1590-2595).
- Billi, A., Presti, D., Faccenna, C., Neri, G., Orecchio, B., 2007. Seismotectonics of the Nubia plate compressive margin in the south Tyrrhenian region, Italy: clues for subduction inception. *J. Geophys. Res.* 112, B08302. <http://dx.doi.org/10.1029/2006JB004837>.
- Billi, A., Presti, D., Orecchio, B., Faccenna, C., Neri, G., 2010. Incipient extension along the active convergent margin of Nubia in Sicily, Italy: Cefal-Etna seismic zone. *Tectonics* 29 (4) (n. TC4026).
- Billi, A., Faccenna, C., Bellier, O., Minelli, L., Neri, G., Piromallo, C., Presti, D., Scrocca, D., Serpelloni, S., 2011. Recent tectonic reorganization of the Nubia-Eurasia convergent boundary heading for the closure of the western Mediterranean. *Bull. Soc. Geol. Fr.* 182, 279–303. <http://dx.doi.org/10.2113/gssgfbull.182.4.279>.
- Bonforte, A., Catalano, S., Maniscalco, R., Pavano, F., Romagnoli, G., Sturiale, G., Tortorici, G., 2015. Geological and geodetic constraints on the active deformation along the northern margin of the hyblean plateau (SE sicily). *Tectonophysics* 640, 80–89. <http://dx.doi.org/10.1016/j.tecto.2014.11.024>.
- Boschi, E., Guidoboni, E., Ferrari, G., Valensise, G., Gasperini, P., 1997. Catalogo dei forti terremoti in Italia dal 461 A.C. al 1990. Istituto Nazionale di Geofisica, Roma (644 pp).
- Camarda, M., De Gregorio, S., Di Martino, R.M.R., Favara, R., 2016. Temporal and spatial correlations between soil CO<sub>2</sub> flux and crustal stress. *J. Geophys. Res. Solid Earth* 121 (10), 7071–7085.
- Cammarata, L., Gambino, S., Maiolino, V., Messina, A., Rapisarda, S., Scaltrito, A., Zuccarello, L., 2014. Contributo delle reti sismiche mobili durante i periodi di crisi: L'esempio della sequenza dei monti Nebrodi del 2011. *Rapporti Tecnici INGV n° 287*. (ISSN 2039-7941).
- Cannata, A., Alparone, S., Ursino, A., 2013. Repeating volcano-tectonic earthquakes at Mt. Etna volcano (Sicily, Italy) during 1999–2009. *Gondwana Res.* 24, 1223–1236.
- Catalano, S., Cinque, A., 1995. L'evoluzione neotettonica dei Peloritani settentrionali (Sicilia nord-orientale): il contributo di una analisi geomorfologica preliminare. *Studi Geol. Camerti* 113–123 (Vol. Spec. 1995/2).
- Catalano, S., Di Stefano, A., 1997. Sollevamento e tettonogenesi Pleistocenica lungo il margine tirrenico dei Monti Peloritani: integrazione dei dati geomorfologici, strutturali e biostratigrafici. *Il Quaternario* 10, 337–342.
- Catalano, S., De Guidi, G., Monaco, C., Tortorici, G., Tortorici, L., 2008. Active faulting and seismicity along the Siculo-Calabrian rift zone. *Tectonophysics* 453, 177–192.
- Catalano, S., Pavano, F., Romagnoli, G., Tortorici, G., 2011. The role of mantle diapirism in the Late Quaternary tectonics and dynamics of eastern Sicily. *GNGTS 30° Convegno Nazionale, Trieste 14–17 Novembre 2011*. Consiglio Nazionale delle Ricerche. Riassunti estesi delle comunicazioni. pp. 117–122.
- Catalano, S., Cirrincione, R., Mazzoleni, P., Pavano, F., Pezzino, A., Romagnoli, G., Tortorici, G., 2017a. The effect of a Meso-Alpine collision event on the tectono-metamorphic evolution of the Peloritani mountain belt (eastern Sicily, southern Italy). *Geol. Mag.* 1–16. <http://dx.doi.org/10.1017/S0016756817000413>.
- Catalano, S., Pavano, F., Romagnoli, G., Tortorici, G., Tortorici, L., 2017b. Late Tortonian–Quaternary tectonic evolution of central Sicily: the major role of the strike-slip deformation. *Geol. Mag.* 1–13. <http://dx.doi.org/10.1017/S0016756817000528>.
- Cello, G., Guerra, I., Tortorici, L., Turco, E., Scarpa, R., 1982. Geometry of the neotectonics stress field in southern Italy: geological and seismological evidence. *J. Struct. Geol.* 4, 385–393.
- Chiarabba, C., Palano, M., 2017. Progressive migration of slab break-off along the southern Tyrrhenian plate boundary: constraints for the present day kinematics. *J. Geodyn.* 105, 51–61.
- Dewey, J.F., Helman, M.L., Turco, E., Hutton, D.H.W., Knott, S.D., 1989. Kinematics of the western Mediterranean. *Alpine Tectonics. Geol. Soc. Spec. Publ.* 45, 265–283.
- Doglioni, C., 1993. Geological evidence for a global tectonic polarity. *J. Geol. Soc. Lond.* 150, 991–1002.
- Doglioni, C., Innocenti, F., Mariotti, G., 2001. Why Mt. Etna? *Terra Nova* 13, 25–31.
- Faccenna, C., Becker, T.W., Lucente, F.P., Jolivet, L., Rossetti, F., 2001. History of subduction and back-arc extension in the Central Mediterranean. *Geophys. J. Int.* 145 (3), 809–820.
- Faccenna, C., Molin, P., Orecchio, B., Olivetti, V., Bellier, O., Funicello, F., Minelli, L., Piromallo, C., Billi, A., 2011. Topography of the Calabria subduction zone (southern Italy): clues for the origin of Mt. Etna. *Tectonics* 30, TC1003. <http://dx.doi.org/10.1029/2010TC002694>.
- Ferranti, L., Antonioli, F., Anzidei, M., Monaco, C., Stocchi, P., 2010. The timescale and spatial extent of vertical tectonic motions in Italy: insights from relative sea-level changes studies. *J. Virtual Explor.* 36. <http://dx.doi.org/10.3809/jvirtex.2009.00255>.



- Finetti, I.R., Lentini, F., Carbone, S., Catalano, S., Del Ben, A., 1996. Il Sistema Appennino Meridionale-Arco Calabro-Sicilia nel Mediterraneo centrale: studio geologico-geofisico. *Boll. Soc. Geol. Ital.* 115, 529–559.
- Frohlich, C., 1992. Triangle diagrams: ternary graphs to display similarity and diversity of earthquake focal mechanisms. *Phys. Earth Planet. Inter.* 75, 193–198. [http://dx.doi.org/10.1016/0031-9201\(92\)90130-N](http://dx.doi.org/10.1016/0031-9201(92)90130-N).
- Gambino, S., Milluzzo, V., Scaltrito, A., Scarfi, L., 2012. Relocation and focal mechanisms of earthquakes in the south-central sector of the Aeolian Archipelago: new structural and volcanological insights. *Tectonophysics* 524–525, 108–115.
- Ghisetti, F., Vezzani, L., 1982. The recent deformation mechanisms of the Calabrian Arc. *Earth Evol. Sci.* 3, 197–206.
- Ghisetti, F., Pezzino, A., Atzori, P., Vezzani, L., 1991. Un approccio strutturale per la definizione della Linea di Taormina: risultati preliminari. *Mem. Soc. Geol. Ital.* 47, 273–289.
- Giammanco, S., Palano, M., Scaltrito, A., Scarfi, L., Sortino, F., 2008. Possible role of fluid overpressure in the generation of earthquake swarms in active tectonic areas: the case of the Peloritani Mts. (Sicily, Italy). *J. Volcanol. Geotherm. Res.* 178 (4), 795–806.
- Giunta, G., Luzio, D., Agosta, F., Calò, M., Di Trapani, F., Giorgianni, A., Oliveri, E., Orioli, S., Pernicaro, M., Vitale, M., Chiodi, M., Adelfio, G., 2009. An integrated approach to investigate the seismotectonics of northern Sicily and southern Tyrrhenian. *Tectonophysics* 476, 13–21. <http://dx.doi.org/10.1016/j.tecto.2008.09.031>.
- Goes, S., Giardini, D., Jenny, S., Hollenstein, C., Kahle, H.G., Geiger, A., 2004. A recent reorganization in the south-central Mediterranean. *Earth Planet. Sci. Lett.* 226, 335–345.
- Got, J.L., Fréchet, J., Klein, F.W., 1994. Deep fault plane geometry inferred from multiplet relative relocation beneath the south flank of Kilauea. *J. Geophys. Res.* 99, 15375–15386.
- Green, D., Neuberg, J., 2006. Waveform classification of volcanic low frequency swarms and its implication. *J. Volcanol. Geotherm. Res.* 153, 51–63.
- Gueguen, E., Tavarneili, E., Renda, P., Tramutoli, M., 2002. The geodynamics of the southern Tyrrhenian Sea margin as revealed by integrated geological, geophysical and geodetic data. *Boll. Soc. Geol. Ital.* 1 (1), 77–85.
- Guidoboni, E., Ferrari, G., Mariotti, D., Comastri, A., Tarabusi, G., Valensise, G., 2007. CFTI4Med, Catalogue of Strong Earthquakes in Italy (461 B.C.–1997) and Mediterranean Area (760 B.C.–1500). INGV-SGA. <http://storing.ingv.it/cfti4med/>.
- Gvirtzman, Z., Nur, A., 1999. The formation of Mount Etna as the consequence of slab rollback. *Nature* 401, 782–785.
- Hirn, A., Nercessian, A., Sapin, M., Ferrucci, F., Wittlinger, G., 1991. Seismic heterogeneity of Mt Etna: structure and activity. *Geophys. J. Int.* 105, 139–153. <http://dx.doi.org/10.1111/j.1365-246X.1991.tb03450.x>.
- Hollenstein, Ch., Kahle, H.G., Geiger, A., Jenny, S., Goes, S., Giardini, D., 2003. New GPS constraints on the Africa–Eurasia plate boundary zone in southern Italy. *Geophys. Res. Lett.* 30. <http://dx.doi.org/10.1029/2003GL017554>.
- ISiDe Working Group (INGV), 2010. Italian Seismological Instrumental and Parametric Database. <http://iside.rm.ingv.it>.
- Jolivet, L., Faccenna, C., Goffé, B., Mattei, M., Rossetti, F., Brunet, C., Storti, F., Funicello, R., Cadet, J.P., D'Agostino, N., Parra, T., 1998. Midcrustal shear zones in postorogenic extension: example from the northern Tyrrhenian Sea. *J. Geophys. Res. Solid Earth* 103 (6), 12123–12160.
- Lahr, J.C., 1989. HYPOELLIPSE/VERSION 2.0: a computer program for determining local earthquake hypocentral parameters, magnitude, and first motion pattern. In: U.S. Geol. Survey, Open-File Report 89/116, (81 pp).
- Lavecchia, G., Ferrarini, F., de Nardis, R., Visini, F., Barbano, M.S., 2007. Active thrusting as a possible seismogenic source in Sicily (Southern Italy): some insights from integrated structural-kinematic and seismological data. *Tectonophysics* 445, 145–167.
- Lentini, F., Catalano, S., Carbone, S., 2000. Nota illustrativa della Carta geologica della Provincia di Messina (Sicilia Nord-Orientale), scala 1:50.000. S.E.L.CA: (Firenze; 70 pp).
- Lickorich, W.H., Grasso, M., Butler, R.W.H., Argnani, A., Maniscalco, R., 1999. Structural styles and regional tectonic setting of the “Gela Nappe” and frontal part of the Maghrebian thrust belt in Sicily. *Tectonics* 18, 655–668.
- Lippitsch, R., White, R., Soosalu, H., 2005. Precise hypocenter relocation of micro-earthquakes in a high-temperature geothermal field: the Torfajökull central volcano, Iceland. *Geophys. J. Int.* 160, 371–388.
- Malinverno, A., Ryan, W.B.F., 1986. Extension in the Tyrrhenian Sea and shortening in the Apennines as result of arc migration driven by slab sinking in the lithosphere. *Tectonics* 5, 227–245.
- Mariotti, D., 1995. An unknown destructive earthquake in 18th century Sicily. In: E. Boschi, R. Funicello, E. Guidoboni and A. Rovelli (eds.), *Earthquakes in the past: multidisciplinary approaches*. *Ann. Geofis.* 38 (5–6), 551–554.
- Miller, S.A., Collettini, C., Chiaraluce, L., Cocco, M., Barchi, M., Kaus, B.J.P., 2004. Aftershocks driven by a high-pressure CO<sub>2</sub> source at depth. *Nature* 427 (6976), 724–727.
- Musumeci, C., Scarfi, L., Palano, M., Patané, D., 2014. Foreland segmentation along an active convergent margin: new constraints in southeastern Sicily (Italy) from seismic and geodetic observations. *Tectonophysics* 630, 137–149. <http://dx.doi.org/10.1016/j.tecto.2014.05.017>.
- Neri, G., Oliva, G., Orecchio, B., Presti, D., 2006. A possible seismic gap within a highly seismogenic belt crossing Calabria and eastern Sicily, Italy. *Bull. Seismol. Soc. Am.* 96 (4A), 1321–1331. <http://dx.doi.org/10.1785/0120050170>.
- Orecchio, B., Aloisi, M., Cannavò, F., Palano, M., Presti, D., Pulvirenti, F., Totaro, C., Siligato, G., Neri, G., 2017. Present-day kinematics and deformation processes in the southern Tyrrhenian region: new insights on the northern Sicily extensional belt. *Ital. J. Geosci.* 136 (3), 418–433.
- Palano, M., Schiavone, D., Loddo, M., Neri, M., Presti, D., Quarto, R., Totaro, C., Neri, G., 2015. Active upper crust deformation pattern along the southern edge of the Tyrrhenian subduction zone (NE Sicily): insights from a multidisciplinary approach. *Tectonophysics* 657, 205–218.
- Pataca, E., Sartori, R., Scandone, P., 1990. Tyrrhenian basin and Apenninic arcs. Kinematic relations since late Tortonian times. *Mem. Soc. Geol. Ital.* 45, 425–451.
- Pavano, F., 2013. Late Quaternary deformation of NE Sicily from relief and drainage system analysis. *Rend. Online Soc. Geol. Ital.* 29, 134–137.
- Pavano, F., Catalano, S., Romagnoli, G., Tortorici, G., 2012. Dynamics and seismotectonics of NE Sicily. *Rend. Online Soc. Geol. Ital.* 21, 241–243.
- Pavano, F., Romagnoli, G., Tortorici, G., Catalano, S., 2015. Active tectonics along the Nebrodi-Peloritani boundary in northeastern Sicily (Southern Italy). *Tectonophysics* 659, 11. <http://dx.doi.org/10.1016/j.tecto.2015.07.024>.
- Pavano, F., Pazzaglia, F.J., Catalano, S., 2016. Knickpoints as geomorphic markers of active tectonics: a case study from northeastern Sicily (southern Italy). *Lithosphere* 8 (6), 633–648. <http://dx.doi.org/10.1130/L577.1>.
- Pondrelli, S., Salimbeni, S., Ekström, G., Morelli, A., Gasperini, P., Vannucci, G., 2006. The Italian CMT dataset from 1977 to the present. *Phys. Earth Planet. Inter.* 159, 286–303. <http://dx.doi.org/10.1016/j.pepi.2006.07.008>.
- Postpischil, D., 1985. Catalogo dei terremoti italiani dall'anno 1000 al 1980. CNR, P.F. Geodinamica, Graficoop, Bologna. (239 pp).
- Presti, D., Billi, A., Orecchio, B., Totaro, C., Faccenna, C., Neri, G., 2013. Earthquake focal mechanisms, seismogenic stress, and seismotectonics of the Calabrian Arc, Italy. *Tectonophysics*. <http://dx.doi.org/10.1016/j.tecto.2013.01.030>.
- Reasenber, P., Oppenheimer, D., 1985. FPFIT, FPPLOT and FPPAGE: FORTRAN computer programs for calculating and displaying fault plane solutions. In: U.S. Geol. Surv. Open File Rep. 85/739, (109 pp).
- Rovida, A., Camassi, R., Gasperini, P., Stucchi, M., 2011. CPTI11, la versione 2011 del Catalogo Parametrico dei Terremoti Italiani. Milano, Bologna (a cura di). <http://emidius.mi.ingv.it/CPTI>.
- Scandone, P., 1979. Origin of the Tyrrhenian Sea and Calabrian Arc. *Boll. Soc. Geol. Ital.* 98, 27–34.
- Scarfi, L., Langer, H., Scaltrito, A., 2005. Relocation of microearthquake swarms in the Peloritani mountains – implications on the interpretation of seismotectonic patterns in NE Sicily, Italy. *Geophys. J. Int.* 163, 225–237. <http://dx.doi.org/10.1111/j.1365-246X.2005.02720.x>.
- Scarfi, L., Messina, A., Cassisi, C., 2013. Sicily and southern Calabria focal mechanism database: a valuable tool for local and regional stress-field determination. *Ann. Geophys.* 56, 1–16.
- Trua, T., Serri, G., Marani, M.P., 2003. Lateral flow of African mantle below the nearby Tyrrhenian plate: geochemical evidence. *Terra Nova* 15, 433440. <http://dx.doi.org/10.1046/j.1365-3121.2003.00509.x>.
- Vavryčuk, V., 2014. Iterative joint inversion for stress and fault orientations from focal mechanisms. *Geophys. J. Int.* 199 (1), 69–77.
- Waldhauser, F., 2001. HypoDD: a computer program to compute double-difference earthquake locations. U.S. Geol. Surv. Open File Rep. 1–113.
- Waldhauser, F., Ellsworth, W.L., 2000. A double-difference earthquake location algorithm: method and application to the northern Hayward fault. *Bull. Seismol. Soc. Am.* 90, 1353–1368.
- Westaway, R., 1993. Quaternary uplift of southern Italy. *J. Geophys. Res.* 98 (B12), 21,741–21,772.
- Wortel, M.J.R., Spakman, W., 2000. Geophysics - subduction and slab detachment in the Mediterranean-Carpathian region. *Science* 290 (5498), 1910–1917.
- Zoback, M.L., 1992. First- and second-order patterns of stress in the lithosphere: the World Stress Map Project. *J. Geophys. Res.* 97 (B8), 11 703–11 728.